Heliyon 10 (2024) e28140

Contents lists available at ScienceDirect

Heliyon

journal homepage: www.cell.com/heliyon

Case report

Evaluation of the total hydrodynamic energy loss using 4D flow MRI in a case with Fontan failure

Ender Odemis [a,*], Terman Gumus [b], İbrahim Başar Aka [c], Sercin Ozkok [d], Kerem Pekkan [e]

[a] Koc University, Faculty of Medicine, Department of Pediatric Cardiology, Faculty of Biomedical Science and Engineering, Turkey
[b] Koc University, Faculty of Medicine, Department of Radiology, Turkey
[c] İstanbul Bilgi University, Faculty of Engineering and Natural Sciences, Department of Mechatronics Engineering, Turkey
[d] Koc University, Faculty of Biomedical Science and Engineering, Turkey
[e] Koc University, Faculty of Engineering Department of Mechanical Engineering, Turkey

ARTICLE INFO

Keywords:
4D flow MRI
Fontan
Cardiac MRI
Energy dissipation
Hemodynamics

ABSTRACT

Fontan Failure (FF) is a common problem for single-ventricle patients as they reach adulthood. Although several mechanisms may cause FF, an optimized blood flow stream through the surgical conduits is essential to avoid excessive energy loss (EL). Recent clinical studies showed EL is related to the quality of life, exercise capacity, and hepatic function since the single-ventricle feeds pulmonary and systemic circulation serially. 4D flow MRI effectively estimates EL in Fontan circulation and allows clinicians to compare the effectiveness of the treatment strategy concerning pre-intervention. Here, we present 26-year-old women with FF who had normal cardiac catheterization findings and were treated according to high EL definitions that are measured through 4D flow MRI.

1. Introduction

Fontan operation is an established palliation strategy in patients with single ventricle physiology. However, it is associated with reduced quality of life due to the gradually declining hemodynamic function with low mortality and morbidity [1]. Therefore, the number of patients with failed Fontan circulation reaching adulthood has increased over time. The final palliation stage is heart transplantation or device support, with limited availability, where early and accurate diagnosis and treatment of hemodynamic abnormalities is crucial to prevent early mortality [2,3]. Echocardiographic examination, computerized tomography (CT), Magnetic resonance imaging (MRI) and cardiac catheterization are the traditional tools for the assessment of the Fontan circulation [1,4,5]. As such, evaluation of the pulmonary artery anatomy, pressure levels, resistances of the Fontan circulation, and systolic and diastolic functions of the single ventricle are essential to reveal the underlying mechanism of the Fontan failure (FF). However, in many cases, these conventional methods are inefficient in conclusively pinpointing the cause of Fontan's failure [2].

Total energy loss (EL) is an emerging clinical hemodynamic parameter representing the pulsatile energy lost due to the blood flow as it flows through the cardiovascular component volume. It is utilized routinely in the pre-surgical planning of Fontan conduits [6]. 4D flow MRI is a useful tool to estimate the EL in the Fontan system and can explain the cause of FF [7]. The clinical importance of EL

* Corresponding author.
E-mail addresses: odemisender@gmail.com (E. Odemis), tgumus@kuh.ku.edu.tr (T. Gumus), basar.aka@bilgi.edu.tr (İ.B. Aka), sercinbas2005@gmail.com (S. Ozkok), kpekkan@ku.edu.tr (K. Pekkan).

https://doi.org/10.1016/j.heliyon.2024.e28140
Received 22 May 2023; Received in revised form 25 February 2024; Accepted 12 March 2024
Available online 13 March 2024

has recently become evident due to its direct influence on exercise capacity and quality of life [8,9]. Here, we present a case with FF presenting with severe ascites. Although echocardiography and cardiac catheterization show normal findings, an interventional approach was initiated and judged according to the comparative EL levels calculated with 4D flow MRI [6,8,9].

2. Case report

A 26-year-old woman was admitted to our outpatient clinic with severe abdominal pain and distension, fatigue, and dyspnoea while resting. Her history included a diagnosis of tricuspid atresia and pulmonary atresia and completed to the Fontan circulation by using an extracardiac conduit without fenestration 17 years ago when she was at 9 years of old. Because of desaturation, a Cheatham platinum stent implantation was performed on the left pulmonary artery in another center 4 years ago.

Two months ago, ascites had been detected and ascites fluid collected at the peritoneal space was drained by using a needle puncture. However, all the symptoms, including ascites, reappeared within a short time. In her echocardiographic examination, the main ventricle is the morphologic left ventricle with normal systolic functions and minimal mitral regurgitation. Blood flow velocities in the superior vena cava and inferior vena cava were normal at 0.8 m/s and 0.7 m/s, respectively. In cardiac catheterization, pulmonary artery pressure was 16 mmHg, and there was no pressure gradient throughout the implanted stent. Flow was normal in the Fontan pathway without any severe narrowing. The cardiac output was calculated at 2.5 LPM. Pulmonary vascular resistance was 1.8 Wood units. Sizes of the pulmonary arteries were normal according to the patient age and weight. With these measurements, we have considered evaluating the liver associated reasons for the ascites. In her blood tests albumin level was 4.5 g/dl, AST 26 U/L, ALT 26 U/L GGT 68 U/L. In the histological examination of the liver needle biopsy, a mild fibrotic process was detected but was not consistent

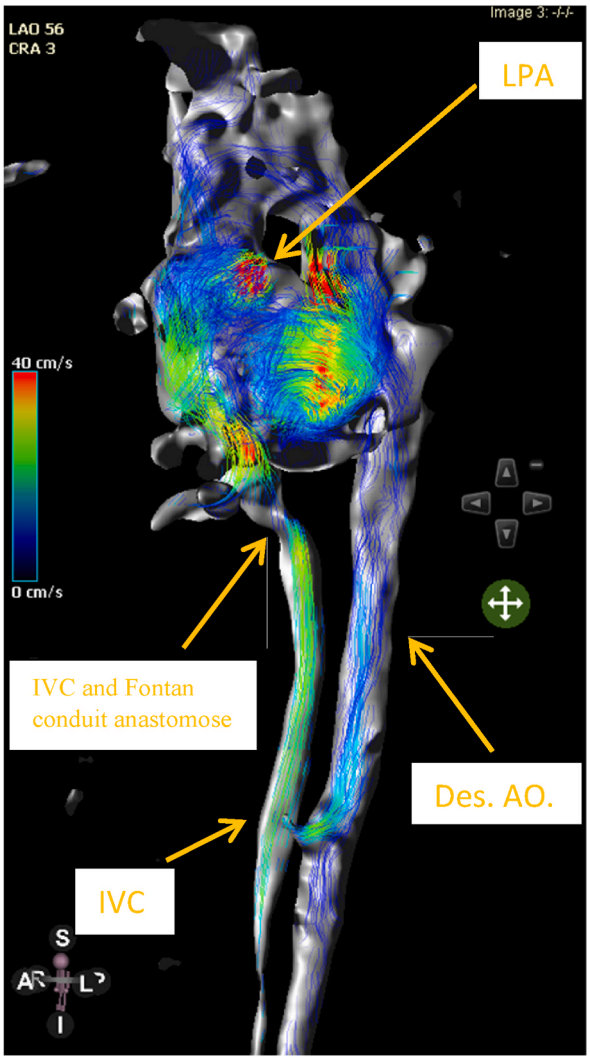

Fig. 1. 4D flow MRI map shows a high velocity at the Fontan conduit close to the origin of left pulmonary artery indicated by arrows. Anatomical parts of the Fontan circulation.

with cirrhosis. With these findings, we decided to re-evaluate the Fontan system since cirrhosis was excluded.

2.1. Cardiovascular Magnetic Resonance Imaging (MRI)

4D flow MRI and conventional sequences were obtained using a 3 T clinical scanner (Vida, Siemens Healthineers, Forchheim, Germany). Image analysis was performed with Circle CVI42, version 5.13 (Circle Cardiovascular Imaging Inc., Calgary, Canada). Before the calculations, 4D flow data quality assurance checks were done. After segmentation of the Fontan circulation pathway, 4D Flow MRI maps were created and measurements were made via following acquisition parameters: Temporal resolution: 50 milliseconds/frame Spatial resolution: 2.5 x 2.5 × 2.8 mm. VENC: 150 cm/s. The ventricular volume was calculated at end-diastolic and end-systolic phases using semi-automated tracing of the endocardial border in all slices and phases in the short axis images. Papillary muscles were included in the ventricular volume. Left ventricle systolic functions were normal, EF: %58 EDV: 133 ml, ESV: 61ml/.

The hydrodynamic dissipation term from the governing Navier-Stokes and energy equation were used to calculate the energy loss (EL) from 4D Flow MRI data. Corresponding EL distribution maps were created using a third-party software (Circle CVI42, v. 5.13). EL and flow velocity components were reported as absolute values, respectively in mW and cm/s.

In streamline and vector fields maps, disturbed flow was detected at the two segments of the Fontan circulation. One at the anastomoses of the inferior vena cava and extracardiac tube, and one at the proximal segment of a previously inserted stent in the LPA (Fig. 1). 3D MRI images of the patient IVC-Fontan anastomosis is shown (Fig. 2a). At the inferior vena cava and extracardiac tube anastomosis, the flow velocity reached 48 cm/s (Fig. 2b and c). In the proximal segment of the previously implanted stent, a velocity increased up to 128 cm/s (Figs. 1 and 2b). Flow through the Fontan pathway is characterized as 'disturbed flow' instead of "turbulent" to illustrate its transitionary flow nature as explained in our earlier work [10,11]. The map of energy loss showed noticeable hot spots in the same segments. A hot spot is defined qualitatively, if the EL is increased relative to its neighboring EL values through a noticeable steep gradient. Energy loss measurements were made at these two locations. At the anastomosis site with the inferior vena cava, EL was 0.08 mW in the mid-diastole (Fig. 3). EL at the proximal segment of the previously inserted stent in LPA was 0.9 mW. According to these findings, most of the total viscous energy loss is attributed to those two regions of the Fontan pathway. According to these findings, we have decided to perform dilatation on these two locations of the Fontan system.

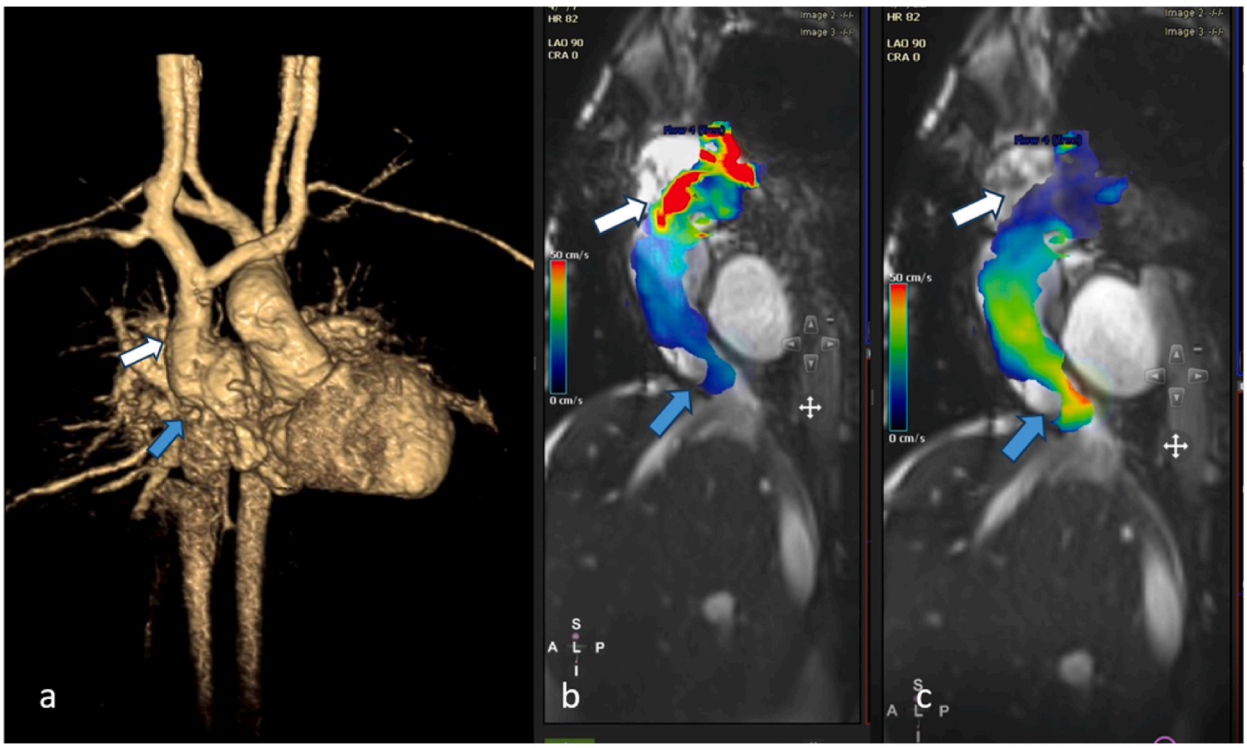

Fig. 2. MRI analysis sequence snapshots for this patient are provided. Increased blood flow velocity at the two sites of the Fontan circulation was observed as red color coded regions. Proximity of these regions correspond to high spatial velocity gradients (a) 3D MRI images of the patient IVC-Fontan anastomosis is marked with blue arrow and Fontan tube is marked with white arrow. Markers indicate the high flow velocity values quantitatively. (b) Disturbed, unstable blood flow encoded in red color at the site of the left pulmonary artery and Fontan tube connection (white arrow) (c) Flow across the inferior vena cava also reported high velocity values (blue arrow).

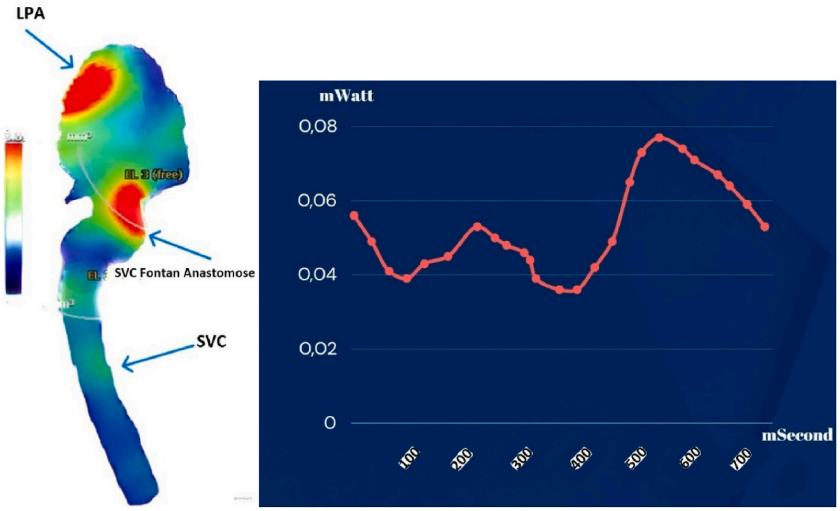

Fig. 3. Energy loss analysis sequence snapshots for this patient are provided. Maximal estimated energy loss detection at IVC and Fontan conduit anastomose and at the origin of the left pulmonary artery are analyzed through the 4D flow MRI velocity measurements. Analysis volumes and regions are displayed in this image.

2.2. Interventional procedure and patient follow-up

Under general anesthesia, hemodynamic measurements were performed. Pulmonary artery and Fontan pressures were measured as 16 mm Hg without a noticeable pressure gradient throughout the stent. Although measurements of the pulmonary artery were not smaller than the stented part of the pulmonary artery, we have decided to implant a stent proximal to the previous stent, as it corresponds to the high-EL region in the 4D flow MRI map. A 21-mm Andra XL stent was implanted using an 18-x-40-mm Z-med balloon (Fig. 4a and b). We have also decided to perform balloon dilatation on the IVC-conduit anastomosis line, where the second location of intense EL was reported. A Z-med high-pressure balloon measuring 16 mm by 30 mm in size was used for the dilatation (Fig. 4c).

One day later, the patient was discharged, and one week later, after the procedure, the ascites disappeared completely. The saturation level of the patient increased to 90 %. There was no recurrent ascites found during the three-month follow-up. Weight loss of 5 kg was observed and linked to ascites. Following the procedure, we performed a control MRI.

2.3. Comparison of 4D flow MRI data before and after the procedure

Anatomical segmentation of the geometry before stent implantation was created (Fig. 5a). The arrows show the IVC-Fontan tube connection and LPA before and after successful re-stent implantation in the left pulmonary artery (Fig. 5b and c) and balloon dilatation of the anastomoses of IVC-Conduit flow conduit region, velocity maps reduced significantly. Map of the EL indicated higher energy loss values at the same segments of Fontan circulation, which disappeared after the interventional procedure (Fig. 5c) Sum of total energy

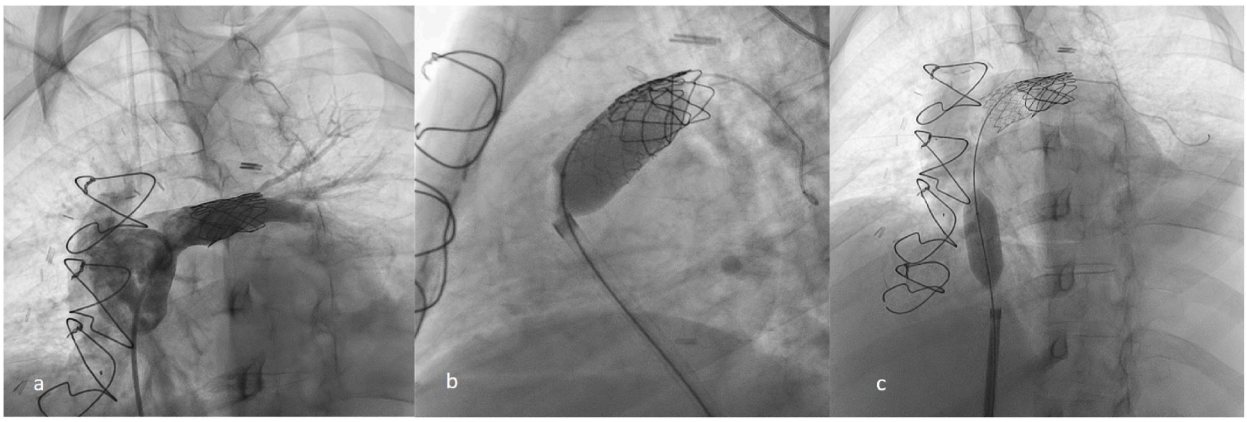

Fig. 4. Interventional procedures are illustrated in steps using the selected angiogram images. (a) Normal appearance of the left pulmonary artery flow at the start of the operation (b) CP stent implantation into the left pulmonary artery (c) Balloon dilation of the inferior vena cava and Fontan conduit.

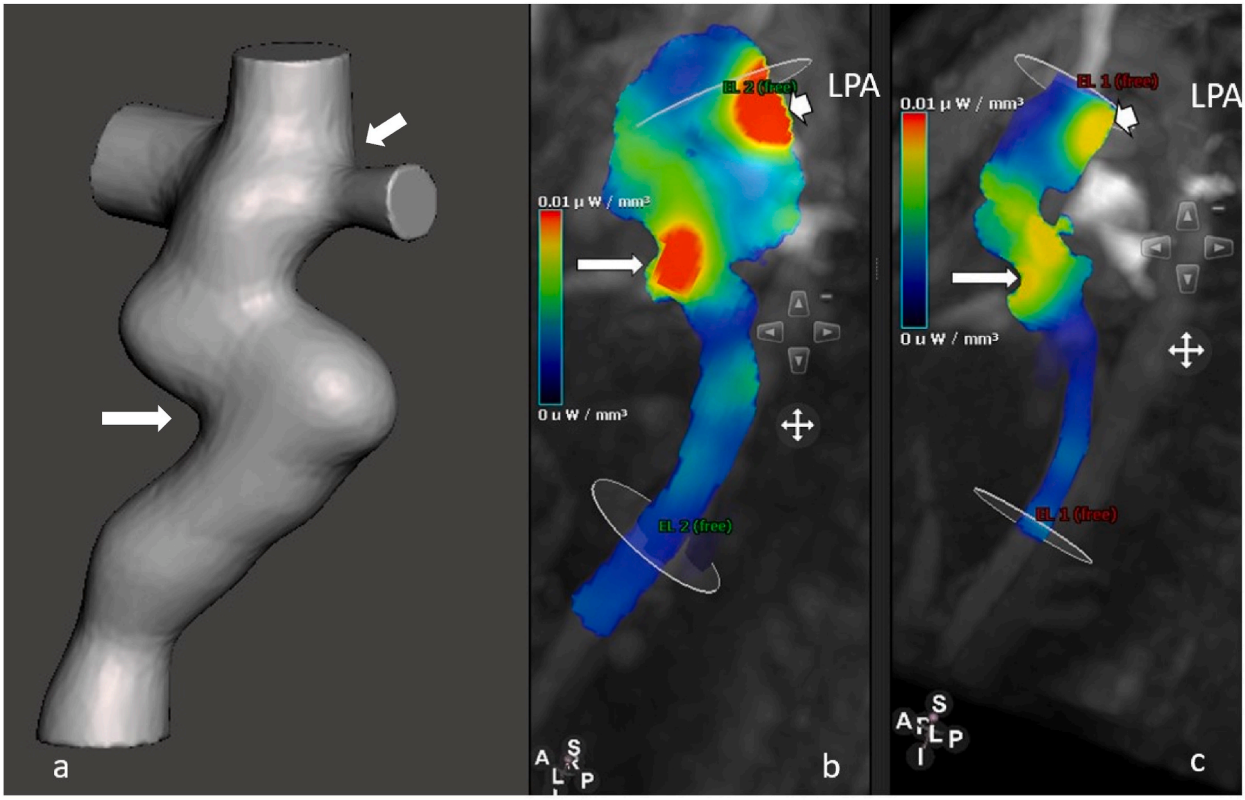

Fig. 5. Pre- and post-intervention 4D flow MRI viscous energy loss maps are compared at the same region of interest (ROI). Figure (a) Anatomical segmentation of the geometry before stent implantation. The arrows show the IVC-Fontan tube connection and LPA (b) The preoperative image indicates higher viscous energy loss levels at the anastomoses site of the IVC-conduit as well as at the location of the stent at the left pulmonary artery. Indicated by white arrows. (c) The corresponding postoperative image shows the removal of the pre-interventional high viscous energy loss sources after re-stenting the left pulmonary artery and balloon dilatation of anastomoses site of IVC-Conduit. Indicated by white arrows.

loss was calculated at the anastomosis site with the inferior vena cava; EL was 0.05 mW in the mid-diastole. EL at the proximal segment of the previously inserted stent in LPA was 0.27 mW.

2.4. CFD analysis of fontan circulation

We aimed to validate our results of the 4D MRI study in Fontan circulation by conducting a Computational Fluid Dynamics (CFD) analysis with a focus on stenotic areas in the Left Pulmonary Artery (LPA) and Inferior Vena Cava (IVC)-Fontan anastomosis regions.

Our study was initiated by extracting patient-specific geometry from Magnetic Resonance Imaging (MRI) data. The segmentation process involved accurately delineating anatomical structures, ensuring a realistic representation of the patient's Total cavopulmonary connection (TCPC). We modified the segmented geometry to virtually model the stent's placement in the left pulmonary artery to match post-interventional measurements in the CAD software environment, thus preparing the geometries for a comparative CFD analysis of both scenarios.

A RANS model utilizing transient calculations is employed within the commercial computational fluid dynamics (CFD) software Fluent 2020 R2 (Ansys, USA). We generated a high-quality mesh to discretize the geometry. We divided the 3D geometries into regions and applied a polyhedral structure to each with consistent accuracy. The mesh structure has a minimum element size of 2.5×10^{-4} m, a maximum element size of 1.25×10^{-3} m, and the number of boundary layers was 5. The pre-intervention geometry comprises 814610 elements, whereas the post-intervention geometry comprises 605636 elements(Fig. 6a). The dimensionless wall distance was $\gamma+<3$ for boundary layers in both models. Boundary conditions were obtained from cardiac catheterization data and MRI flow studies. The IVC and SVC were configured with inlet velocities of 0.7 m/s and 0.8 m/s, respectively, while the pressure outlets were 16 mmHg at the pulmonary artery.

The blood was modelled as an incompressible Newtonian fluid with a density of 1050 kg/m^3 and a viscosity of 0.0035 Pa s. We assessed flow velocities, flow ratios, wall shear stress, pressure drop, and energy loss. The k-omega SST model was employed to conduct a transient analysis, which integrated specified boundary conditions for evaluating calculations. Time step size was was set to 0.005s for 1000 time steps. Flow rates from the IVC and SVC to the pulmonary arteries were determined individually using User-Defined Scalars. Subsequently, a transient analysis was run to model pulsatile blood flow by loading a User-Defined Function

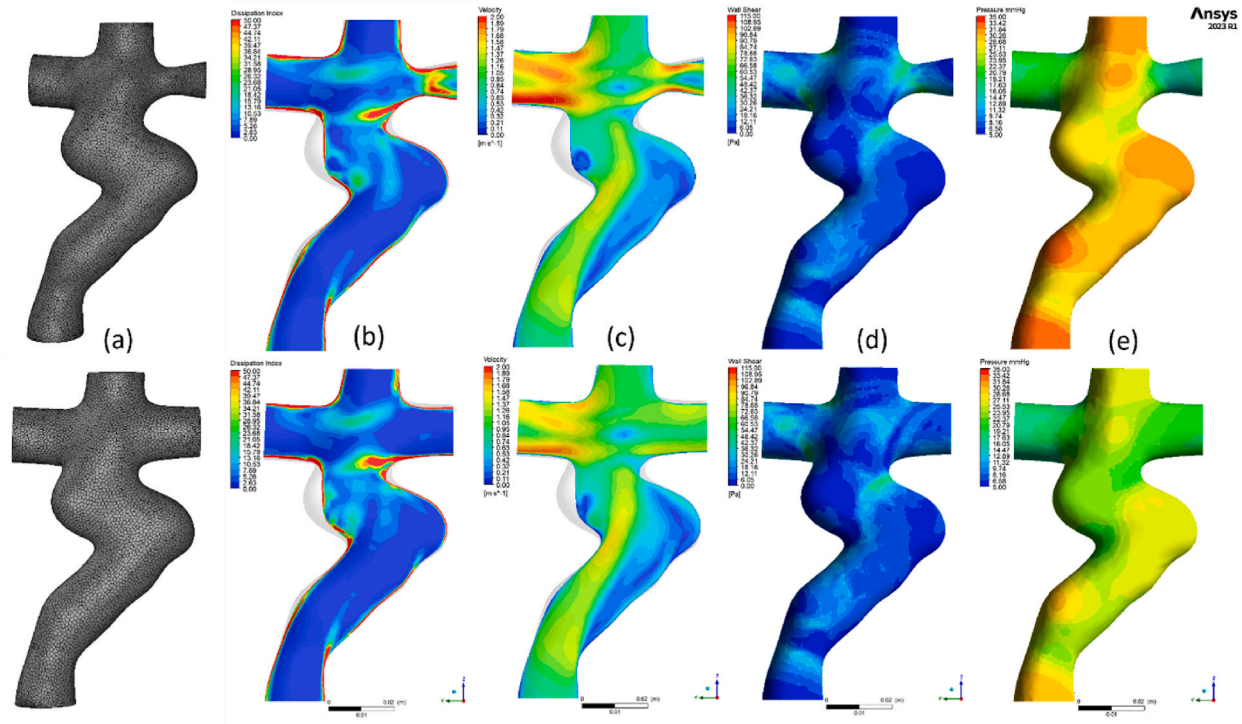

Fig. 6. Pre and post-interventional geometries were meshed (a). A normalized dissipation index was calculated for visualization of high energy loss regions where there is a significant drop after the intervention (b). Velocity profiles were visualized where the intervention reduced the high velocity flow in LPA (c). Wall shear stress was also displayed to show the decrease after the intervention around LPA (d). Similarly, the pressure drop was visualized (e).

(UDF) that defined Windkessel resistance for the outlets and included an inlet velocity profile [11]. A convergence residual of 10^{-5} was determined as the convergence criterion along with a steady pressure value at the outlets.

The pre and post-intervention energy loss, total pressure drop, and flow ratios were reported in Table 1. To ensure the credibility of our CFD results, we compared our findings with 4D flow MRI data obtained independently. The consistency observed between the CFD analysis, and 4D flow MRI results served as a validation of the accuracy of our computational model. These findings provide a comprehensive understanding of the hemodynamic characteristics of the patient's unique physiology.

3. Discussion

Given that the single-ventricle is in charge of both the systemic and pulmonary circulations, it is imperative to preserve as much of the hydrodynamics energy of the blood that travels through the Fontan circulation as possible. As a result, several *in vitro*, numerical, and *in vivo* investigations have been conducted to examine the fluid mechanical optimization of the Fontan conduit D(FC) [1,12]. Mechanical energy loss can be calculated by obtaining the pressures and flows from the left pulmonary artery (LPA), right pulmonary artery (RPA), superior vena cava (SVC), and inferior vena cava (IVC). In a clinical setting, its accuracy is arguable since the pressure measurements from these locations are related to catheter localization and are prone to movement artifacts [13]. Whereas 4D flow MRI allows the calculation of total EL from MRI phase velocity mapping without the need for pressure data. Phase contrast MRI images are useful to reveal flow disturbances in the presence of normal pressure records [14]. The velocity vectors throughout the Fontan circulation make it possible to estimate total energy loss through the viscous dissipation function [13,15]. Still, the accuracy of EL from

Table 1
Flow ratios and energy losses according to computational fluid dynamics results of the model before and after stent implantation are shown.

	$Q_{IVCtoLPA}$ (%)	$Q_{IVCtoRPA}$ (%)	$Q_{SVCtoLPA}$ (%)	$Q_{SVCtoRPA}$ (%)	Energy Loss (mW)	Pressure Drop (mmHg)
Pre - intervention	18.25	82.75	16.62	84.38	8.74	30.19
Post - intervention	53.59	46.41	11.91	88.09	8.32	22.03

$Q_{IVCtoLPA}$: Flow ratio of inferior vena cava flow to left pulmonary artery·
$Q_{IVCtoRPA}$: Flow ratio of inferior vena cava flow to right pulmonary artery·
$Q_{SVCtoLPA}$: Flow ratio of superior vena cava flow to left pulmonary artery·
$Q_{SVCtoRPA}$: Flow ratio of superior vena cava flow to left pulmonary artery·

4D flow MRI largely depends on the MRI sequence resolution and provides only comparative estimates due to the numerical estimation of blood velocity gradients. The Circle system does not differentiate the flow regime whether it is turbulent, laminar, or transitionary. Likewise, the hydrodynamic energy dissipation function formula, provided below, is valid for any flow regime, given through the following mathematical expression [16]:

$$\Phi = 2\mu\left[\left(\frac{\partial u}{\partial x}\right)^2+\left(\frac{\partial v}{\partial y}\right)^2+\left(\frac{\partial w}{\partial z}\right)^2+\frac{1}{2}\left(\frac{\partial u}{\partial y}+\frac{\partial v}{\partial x}\right)^2+\frac{1}{2}\left(\frac{\partial w}{\partial y}+\frac{\partial v}{\partial z}\right)^2+\frac{1}{2}\left(\frac{\partial w}{\partial x}+\frac{\partial u}{\partial z}\right)^2\right] \quad (1)$$

Here *u, v,* and *w* are the three components of the velocity vector. For transient flows (unsteady) the equation [1] is calculated for the specific instant of time, typically at an instant during the cardiac cycle. While the equation is the same for any flow type, the calculation and measurement of these velocity gradients are challenging and can introduce numerical errors depending on how these gradients are approximated numerically. For example, we cannot resolve these gradients correctly for large voxel sizes and miss small flow vortices encountered in turbulent flow. Even though the numerical values are prone to errors, this equation was used in CFD simulations with a UDF to visualize high dissipation regions as a normalized dissipation index by mapping the numerical values in the same range (Fig. 6b). Various levels of spatial and temporal averaging processes employed in 4D flow MRI acquisition also lead to unsynchronized velocity components and gradients. Thus, for highly fluctuating flows, like transitionary/turbulent flow regimes, numerical computation of these gradients will miss important physics and bring a lot of error. Similarly, as a significant portion of the dissipation is from the vessel wall (due to the no-slip condition), the 4D flow MRI typically cannot resolve the wall layer accurately for coarse voxels. On the other hand, if we reduce the voxel size, any small error in velocity gradient computation (differences) will grow/propagate due to the square power in the equation, and this equation will result in wrong values. Even though the equation is valid for any flow regime, the numerical computation of these velocity gradients requires detailed verification, trials with mock-up models, and validation. In Fontan hemodynamics, we prefer to use the "Control Volume" version of the power loss, which requires pressure measurement at the vessel inlet outlets. Still, the energy loss calculated from the velocity gradients will provide "comparative" results and will be useful in interventional planning, as presented in this paper.

Despite this limitation, disturbed flow, related to increased EL Fontan circulation, was shown previously, and an operational strategy was defined accordingly based on the flow vectors [17]. In the presented case, since the pressures at the IVC, SVC, and pulmonary arteries are almost equal, conventional cardiac catheterization cannot detect the Fontan failure mechanism, and 4D flow MRI was employed. The distribution of EL hotspots was visualized through 4D flow MRI, and the change in viscous energy loss between pre- and post-dilation can be reported. The clinical importance of energy loss in Fontan patients has been reported earlier [8,11]. Even a quantum improvement in the Fontan flow and resulting lower El levels may influence the clinical outcome of Fontan circulation. Based on our present knowledge, El is useful as a 'comparative' index judging pre- and post-hemodynamic states, as its absolute levels are challenging to measure, and an optimal interventional procedure cannot be planned according to this data for every patient case. Given these limitations, EL is an emerging clinical index that should be considered. The accuracy of EL from 4D flow MRI needs to be validated *in vitro* using 3D printed mock-up MRI models, but its comparative use is clear in the present application.

It is shown that flow distribution from the inferior vena cava is mainly directed towards the left pulmonary artery (LPA) in the extracardiac Fontan circulation [7]. In the presented case, high EL at the LPA orifice just before the stent LPA would be the predominant mechanism of the patient's inefficient palliation. Additional EL sources were detected at the proximal anastomoses of the extracardiac conduit and inferior vena cava. The geometry of the Fontan circulation directly affects the streamline flow patterns and is closely related to energy loss in the system. In this case, we considered that the dilated and bent conduit is the main reason for increased flow velocity changes, which are associated with high EL and eventually result in ineffective flow to the pulmonary arteries [18–20]. While the EL distributions, possible hot spots, and high EL gradients are well defined throughout the TCPC conduits via the computational fluid dynamic studies, for the 4D flow MRI protocols, significant EL cut-off values are still qualitative, and more work is needed. Thus, in this article, the cut-off values and hot spots are based on visual observations and utilized to compare pre-and post-interventional outcomes.

When we compare our MRI and clinical results with CFD analysis, it is shown that pulmonary blood flow distribution is changed after stent implantation, which is mostly towards the right pulmonary artery before the procedure. There was a significant reduction of velocity in LPA (Fig. 6c). Similarly, pressure and wall shear stress around the LPA region was also reduced significantly (Fig. 6d and e). Additionally, Energy loss calculations by using CFD is also concordant with the results that was obtained by MRI (Fig. 6b). As a result, we can comment that CFD analysis also confirmed our MRI measurements results and clinical improvement.

In conclusion, this case illustrates the clinical importance of the utility of 4D flow MRI to clarify the hemodynamic abnormalities that may cause FF, particularly in cases with normal/equal cardiac catheterization pressures. As a non-invasive technique this approach can potentially replace or support the invasive cardiac catheterization in the evaluation of challenging Fontan circulation cases. Prospective studies are needed to evaluate the dependability and feasibility of this approach in clinical settings.

Ethical standards

Koc University IRB board approved this study to be conducted with an informed consent form obtained from the patient. Any patients whose data or images are included in our publication have consented for all images and clinical data and other data included in the manuscript to be published.

Data availability statement

All authors confirm that all data and materials as well as software application or custom code support their published claims and comply with field standards. Data will be made available on request.

CRediT authorship contribution statement

Ender Odemis: Writing – review & editing, Writing – original draft, Project administration, Methodology, Formal analysis, Data curation, Conceptualization. **Terman Gumus:** Formal analysis, Data curation. **İbrahim Başar Aka:** Writing – review & editing, Software, Formal analysis. **Sercin Ozkok:** Visualization. **Kerem Pekkan:** Writing – review & editing, Writing – original draft, Methodology, Conceptualization.

Declaration of competing interest

The authors declare that they have no known competing financial interests or personal relationships that could have appeared to influence the work reported in this paper.

Acknowledgements

We acknowledge TUBITAK 2247A lead researcher award 120C139 and ERC (European Research Council) Proof of Concept 969765 BloodTurbine providing funding. The Circle CVI company did not respond to the Author's inquiry requesting the details of their hydrodynamic dissipation calculation.

References

[1] J.C. Dykes, D.N. Rosenthal, D. Bernstein, D.B. McElhinney, M.R.K. Chrisant, K.P. Daly, et al., Clinical and hemodynamic characteristics of the pediatric failing Fontan, J. Heart Lung Transplant. 40 (12) (2021) 1529–1539.
[2] A.C. Egbe, H.M. Connolly, W.R. Miranda, N.M. Ammash, D.J. Hagler, G.R. Veldtman, et al., Hemodynamics of fontan failure: the role of pulmonary vascular disease, Circ. Heart Fail 10 (12) (2017).
[3] B. Mondésert, F. Marcotte, F.P. Mongeon, A. Dore, L.A. Mercier, R. Ibrahim, et al., Fontan circulation: success or failure? Can. J. Cardiol. 29 (2013) 811–820.
[4] C.Z. Lam, E.T. Nguyen, S.J. Yoo, R.M. Wald, Management of patients with single-ventricle physiology across the lifespan: contributions from magnetic resonance and computed tomography imaging, Can. J. Cardiol. 38 (2022) 946–962.
[5] C.W. Akins, B. Travis, A.P. Yoganathan, Energy loss for evaluating heart valve performance, J. Thorac. Cardiovasc. Surg. 136 (4) (2008) 820–833.
[6] S.S. Lashkarinia, M. Cicek, B. Kose, M. Rezaeimoghaddam, E.H. Yılmaz, N.A. Aydemir, et al., A novel Fontan Y-graft for interrupted inferior vena cava and azygos continuation, Interact. Cardiovasc. Thorac. Surg. 34 (6) (2022) 1095–1105.
[7] K.S. Sundareswaran, C.M. Haggerty, D. de Zélicourt, L.P. Dasi, K. Pekkan, D.H. Frakes, et al., Visualization of flow structures in Fontan patients using 3-dimensional phase contrast magnetic resonance imaging, J. Thorac. Cardiovasc. Surg. 143 (5) (2012) 1108–1116.
[8] E. Tang, Z. Wei, K.K. Whitehead, R.H. Khiabani, M. Restrepo, L. Mirabella, et al., Effect of Fontan geometry on exercise haemodynamics and its potential implications, Heart 103 (22) (2017) 1806–1812.
[9] Mercer-Rosa L, Fogel MA, Wei A, Trusty PM, Tree M, Tang E, et al. Fontan Geometry and Hemodynamics Are Associated with Quality of Life in Adolescents and Young Adults.
[10] K.S. Sundareswaran, K. Pekkan, L.P. Dasi, K. Whitehead, S. Sharma, K.R. Kanter, et al., The total cavopulmonary connection resistance: a significant impact on single ventricle hemodynamics at rest and exercise the total cavopulmonary connection resistance: a significant impact on single ventricle hemodynamics at rest and exercise [Internet], Am. J. Physiol. Heart Circ. Physiol. 295 (2008) 2427–2435.
[11] C. Wang, K. Pekkan, D. de Zélicourt, M. Horner, A. Parihar, A. Kulkarni, A.P. Yoganathan, Progress in the CFD modeling of flow instabilities in anatomical total cavopulmonary connections, Ann. Biomed. Eng. 35 (11) (2007) 1840–1856.
[12] R.H. Khiabani, K.K. Whitehead, D. Han, M. Restrepo, E. Tang, J. Bethel, et al., Exercise capacity in single-ventricle patients after Fontan correlates with haemodynamic energy loss in TCPC, Heart 101 (2) (2015) 139–143.
[13] A.K. Venkatachari, S.S. Halliburton, R.M. Setser, R.D. White, G.P. Chatzimavroudis, Noninvasive quantification of fluid mechanical energy losses in the total cavopulmonary connection with magnetic resonance phase velocity mapping, Magn. Reson. Imaging 25 (1) (2007) 101–109.
[14] D.T. Wymer, K.P. Patel, W.F. Burke, V.K. Bhatia, Phase-contrast MRI: physics, techniques, and clinical applications, Radiographics 40 (1) (2020) 122–140.
[15] T.M. Healy, C. Lucas, A.P. Yoganathan, Noninvasive fluid dynamic power loss assessments for total cavopulmonary connections using the viscous dissipation function: a feasibility study, J. Biomech. Eng. 123 (4) (2001) 317–324.
[16] R. Rasooli, O. Dur, K. Pekkan, Estimation of pulsatile energy dissipation in intersecting pipe junctions using inflow pulsatility indices, AIP Adv. 11 (1) (2021) 015342.
[17] F.M. Rijnberg, H.C. van Assen, M.G. Hazekamp, A.A.W. Roest, Tornado-like Flow in the Fontan Circulation: Insights from Quantification and Visualization of Viscous Energy Loss Rate Using 4D Flow MRI, vol. 40, European Heart Journal. Oxford University Press, 2019, p. 2170.
[18] M.S.M. Elbaz, R.J. van der Geest, E.E. Calkoen, A. de Roos, B.P.F. Lelieveldt, A.A.W. Roest, et al., Assessment of viscous energy loss and the association with three-dimensional vortex ring formation in left ventricular inflow: in vivo evaluation using four-dimensional flow MRI, Magn. Reson. Med. 77 (2) (2017) 794–805.
[19] F.M. Rijnberg, J.F. Juffermans, M.G. Hazekamp, W.A. Helbing, H.J. Lamb, A.A.W. Roest, et al., Segmental assessment of blood flow efficiency in the total cavopulmonary connection using four-dimensional flow magnetic resonance imaging: vortical flow is associated with increased viscous energy loss rate, Eur. Heart J. Open (2) (2021) 1.
[20] K. Pekkan, H.D. Kitajima, D. de Zelicourt, J.M. Forbess, W.J. Parks, M.A. Fogel, S. Sharma, K.R. Kanter, D. Frakes, A.P. Yoganathan, Total cavopulmonary connection flow with functional left pulmonary artery stenosis: angioplasty and fenestration in vitro, Circulation 112 (21) (2005) 3264–3271.